



Effects of post-weld heat treatment on the microstructure and properties of the matching SMAW filler metal for weld joints in MarBN steel

Zhuyao Zhang¹ · Steve Roberts² · Josh Wildgoose² · Will Philpott³ · Mark A. E. Jepson³

Received: 2 October 2023 / Accepted: 30 November 2023 / Published online: 8 February 2024
© The Author(s) 2024

Abstract

A detailed investigation has been carried out of the matching composition filler metal for welding MarBN steel to explore the influence of welding procedure and post-weld heat treatment (PWHT) on the microstructure and properties of the weld metal and a MarBN steel weld joint. The filler metal was in the form of a shielded metal arc welding (SMAW) electrode. With different interpass temperatures and PWHT procedures applied, the microstructure and mechanical properties, particularly toughness, of the all-weld metal deposits and welded MarBN alloy joints were examined. The differences in microstructure (grain structure, precipitates, etc.) were evaluated to provide a better understanding of how the PWHTs influence the starting conditions of the matching weld metal and welded MarBN steel joints before service. The current work found that for a 30-mm-thick all-weld metal coupon, reasonable impact toughness was achieved after PWHT of 735 °C × 8 h; longer heat treatment durations (16 h and 36 h) did not further increase the toughness. For thicker cast blocks, a PWHT of 735 °C × 16 h was needed for weld toughness comparable to the base metal, hence was considered more appropriate for actual engineering applications. Evenly distributed Laves phase precipitation was observed after 735 °C × 8 h; the precipitates gradually increased in size and area fraction as the duration increased, and appeared to be stable when approaching 36 h. Differences in the precipitation were observed between different weld regions. The weld cap region had a lower density of Laves precipitates compared to the lower weld area. From the current investigation, aspects for further investigation are also identified.

Keywords Thermal power · MarBN · IBN-1 · Cr–Mo filler metal · PWHT · Microstructure · Precipitation · Laves · Properties · Toughness

1 Introduction

Since the reports of promising creep properties of MarBN alloys (a short name for Martensitic 9Cr steel strengthened by boron and nitrides), nearly two decades ago [1–3], significant effort has been spent in validating the MarBN base steel, and development of matching filler metals [4–12].

One of the leading candidates for the new advanced alloys is the UK's IBN-1 casting alloy which was developed by Goodwin Steel Castings Limited within the IMPACT project [4]. After the IMPACT project, IBN-1 has been further studied within consecutive UK collaborative research projects, IMPEL [6], IMPULSE [7] and IMPLANT [13], from which this study has originated. IBN-1 currently leads the development in casting materials for applications such as turbine components, etc. and initial study reports indicate clear advances in the creep performance over the CB2 alloy [8]. Figure 1 shows two examples of the cast turbine components fabricated by Goodwin Steel Castings using IBN-1 steel.

One of the main targeted applications of MarBN steel is in castings for turbine components. These applications are likely to involve repair welding of castings and welded joints between castings and other structures, such as cast valves and steam pipe-works, etc. In order to produce welded joints with satisfactory microstructure

Recommended for publication by Commission II - Arc Welding and Filler Metals

✉ Zhuyao Zhang
zzhang@lincolnelectric.eu

¹ Lincoln Electric Europe, Sheffield, UK

² Goodwin Steel Castings Ltd, Stoke-On-Trent ST1 3NR, UK

³ Department of Materials, Loughborough University, Loughborough LE11 3TU, UK

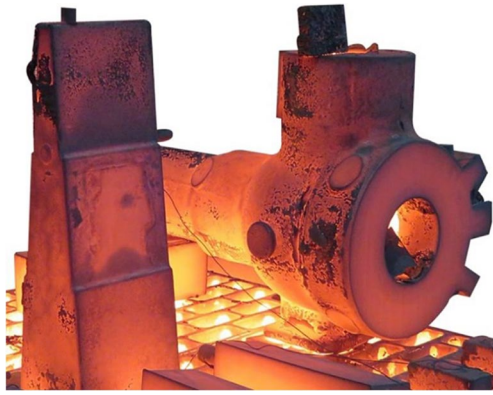


Fig. 1 IBN-1 control valve casting 2050 kg (right) and step block casting 800 kg (left) during cooling after austenitisation [8] (Courtesy of Goodwin Steel Castings Ltd, UK)

and properties, there are practical needs for developing appropriate welding procedures and PWHT parameters. Particularly, a relatively lower PWHT peak temperature, i.e. 735 °C, is preferred for heat treating large scale cast components.

The development of an appropriate PWHT is a balance between the weld's toughness and long-term creep stability throughout the component's service life. The first objective is to ensure that the PWHT creates a material with acceptable toughness and other mechanical properties. However, within MarBN steel, it has been previously shown that a short PWHT of 760 °C × 2 h caused the formation of Laves phase within the HAZ [9]. As the effect of Laves phase on creep behaviour varies with exposure time, where small precipitates can be beneficial and larger particles detrimental [14], it is necessary to understand its formation at the proposed lower PWHT temperature

studied here, in conjunction with the primary objective of obtaining satisfactory mechanical performance.

Within the UK collaborative project, IMPLANT [13], a detailed investigation was carried out on the matching composition filler metal for welding MarBN steel to explore the influence of welding procedure and PWHT on the microstructure and properties of the weld metal and welded joint.

2 Details of materials used for the investigation

2.1 Base metal

Table 1 shows the typical composition of the IBN-1 cast steel. Figure 2 shows a typical microstructure of IBN-1 steel in the normalised and tempered condition, which consists of tempered martensite.

2.2 Filler metal

The filler metal used for the current investigation was in the form of shielded metal arc welding (SMAW) electrode. It is an electrode developed by Lincoln Electric with a product designation of Chromet 933. This basic coated electrode can be classified as AWS A5.5/A5.5 M [15]: E9015-G H4/E6215-G H4 and EN ISO 3580-A [16]: E ZCrWCovNb 9 3 3 B 3 2 H5.

In this study, electrodes of two diameters, 3.2 mm and 4.0 mm, were used. The chemical composition of all-weld metal deposits from the actual batch analyses are listed in Table 2. The values of Cr-Ni balance (CNB) were calculated using the contents of relevant elements. CNB is an index indicating the tendency for δ -ferrite formation [17]. A CNB

Table 1 Typical chemical composition of IBN-1 cast steel (wt. %)

Material	C	Mn	Si	Cr	Mo	Ni	W	Co	V	Nb ^a	B ^b	N
IBN-1	0.10	0.54	0.45	9.0	0.05	0.14	2.5	3.0	0.20	0.06	120	0.020

^aIncluding tantalum

^bB content value is in ppm

Fig. 2 Microstructure of the MarBN steel (IBN-1) consisting of tempered martensite

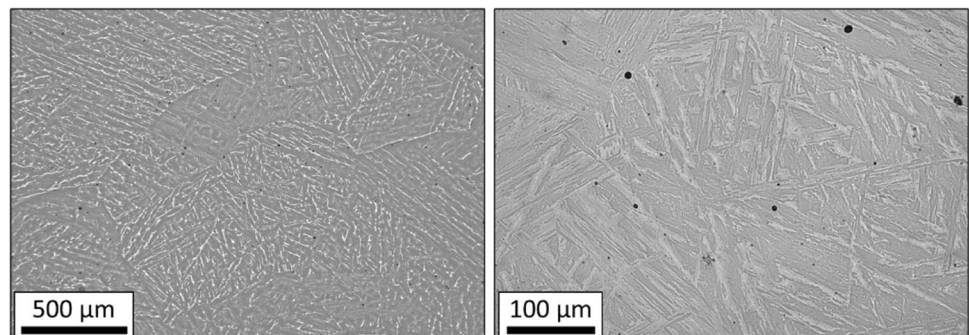


Table 2 Undiluted all-weld deposit composition of the filler metal (wt. %)

Diameter	C ^a	Mn	Si	Cr	Ni	Mo	W	Co	V	Nb	B ^b	Al	N ^a	Cu	CNB ^c
3.2 mm	0.10	0.63	0.17	9.11	0.52	0.36	2.7	2.8	0.22	0.050	78	0.006	0.038	0.07	10
4.0 mm	0.11	0.55	0.22	8.93	0.37	0.36	2.6	3.1	0.22	0.050	79	0.003	0.042	0.05	10

^aC and N contents were measured using LECO; other elements with OES

^bB content value is in ppm

^cCr–Ni balance (CNB) given by modified Newhouse's equation: $CNB = Cr + 6Si + 4Mo + 1.5W + 11V + 5Nb + 9Ti + 12Al - 40C - 30N - 4Ni - 2Mn - 1Cu$ [17]

value of 10 indicates that δ -ferrite is not predicted to be present in these weld metals [18], and this is confirmed by the microstructure examinations.

2.3 Experimental procedure

Assemblies of all-weld metal deposits as well as welded joints made between IBN-1 base alloy plates were prepared. Post-weld heat treatments (PWHTs) with different soaking durations were applied. Ambient temperature mechanical tests were conducted. All-weld metal and cross-weld transverse tensile, impact, hardness and bend properties were assessed. Tensile tests were performed to ASTM E8/E8M-16a [19]. Hardness tests were performed to ASTM E10-18 [20]. Charpy impact testing was performed to ASTM A370-19 [21]. Bend testing was performed to ASTM E190-14 [22] with 38 mm former/65 mm shoulder.

The microstructure of the weld metals after different PWHT procedures were examined using optical microscopy and scanning electron microscopy (SEM). The differences in microstructure (grain structure and precipitates, etc.) were evaluated in order to determine the possible reasons for the differences in mechanical properties, particularly in toughness at ambient temperature.

Metallurgical specimens for optical microscopy examination were ground and final polished to a 1 μm finish and then etched with a Villela etchant solution. Electron microscopy was conducted after preparation of the samples through mounting in electrically conductive Bakelite, grinding and polishing to a finish of 1 μm and a final colloidal silica polish using a Struers Tegramin polishing machine. Electron backscatter diffraction (EBSD) and backscatter electron imaging (BSE) was carried out using the electron column of a ThermoFisher Helios G4 DualBeam pFIB or a JEOL 7100F. For BSE imaging in either instrument, an accelerating voltage of 10 kV was used. No further etching was necessary to reveal the secondary phases described.

Quantification of bright particle phases within the samples was completed using ImageJ by thresholding a set of images (covering at least 1200 μm^2), according to brightness and then measuring their size distribution. From this, the average size was calculated along with the count per unit area and the area fraction of particle coverage. In order

to produce the size distributions, the data were plotted both as number weighted and area weighted distribution. When thresholding the images, particles were required to exceed a size of 6 pixels in an image which equated to an area of $\sim 0.001 \mu\text{m}^2$. The measurement used to determine a particle's size was the Feret diameter which is a measure of the largest length across a 2-dimensional image of a particle. This measurement is also known as the calliper length.

3 Results and discussion

3.1 All-weld metal tests and results

3.1.1 Test assembly preparation and PWHT

All-weld test assemblies were prepared using an electrode of diameter 4.0 mm. The thickness of the coupons prepared were nominally 30 mm. The welding was conducted at PA/1G position. The pre-heat temperature was 200 $^{\circ}\text{C}$, interpass temperature was in the range of 250–300 $^{\circ}\text{C}$ with a typical level of 275 $^{\circ}\text{C}$. The welding parameters used were voltage 24 V and current 135 A giving a heat input of 1.3–1.4 kJ/mm. Limited weaving was applied to approximately 4.0–6.0 mm.

After welding, the weld assemblies were cooled to room temperature to ensure a full martensite transformation, then post-weld heat treated at 735 $^{\circ}\text{C}$ for durations of 2, 4, 8, 16 or 36 h, respectively. The cooling was controlled in such a way that the assemblies were furnace cooled (FC) to 300 $^{\circ}\text{C}$, then followed by an air cool to ambient temperature.

3.1.2 All-weld metal mechanical properties and effect of PWHT

The tensile, hardness and Charpy impact toughness properties of the welds are listed in Table 3.

The results indicate that, at the relatively low PWHT temperature of 735 $^{\circ}\text{C}$, meaningful tempering to the microstructure started after a 4-h hold. The effect reached a significant degree after 8 h holding. This is reflected by the considerable changes in mechanical properties making the weld metal deposit comparable to the IBN-1 base alloy after

Table 3 Mechanical properties of all-weld metals after different PWHT

Material	PWHT	Rp0.2 (MPa)	Rm (MPa)	A (4d) (%)	Z (%)	HBW	CVN at +20 °C (J, avg./ind.)
IBN-1 [8]	Annealed+tempered	625	767	24	60	231	41 (avg.)
All-weld metal	735°Cx2h+FC	910	1008	13.0	38	310	7/7, 7, 7
	735°Cx4h+FC	883	985	14.0	48	285	6/7, 6, 6
	735°Cx8h+FC	651	815	21.0	51	252	38/38, 37, 39
	735°Cx16h+FC	617	799	21.0	55	254	27/22, 26, 34
	735°Cx36h+FC	617	785	20.0	55	241	31/30, 29, 34

avg. average, ind. individual

annealing and tempering. These included tensile strength and ductility, impact toughness as well as hardness. Further increases in holding time to 16 h and 36 h did not produce further considerable changes in properties but did produce a reduction in tensile strength and hardness. The toughness values achieved after PWHT at 735 °C with a holding time above 8 h are very similar to those reported after PWHT at 765 °C for 2 and 4 h with a standard AWS A5.5 all-weld metal classification assembly [15].

3.1.3 Microstructure examination of all-weld metal and effect of PWHT

Figure 3 shows the microstructure of the as-deposited weld metal with a typical fully martensite structure with no sign of any δ -ferrite. This is in a good agreement with the Cr-Ni balance (CNB) value of 10.

Figure 4 shows EBSD maps of the weld metal after PWHT at 735 °C × 8, 16 and 36 h, respectively. EBSD analysis shows a microstructure typical of multi-layer welds with regions of columnar grains aligned perpendicular to the direction of the weld bead, bordered by regions of much smaller and more equiaxed grains. The EBSD maps show no discernible change in the grain structure with different PWHT holding times at this temperature, indicating that the

heat treatment has not altered the general grain structure of the weld metal with increasing time at 735 °C.

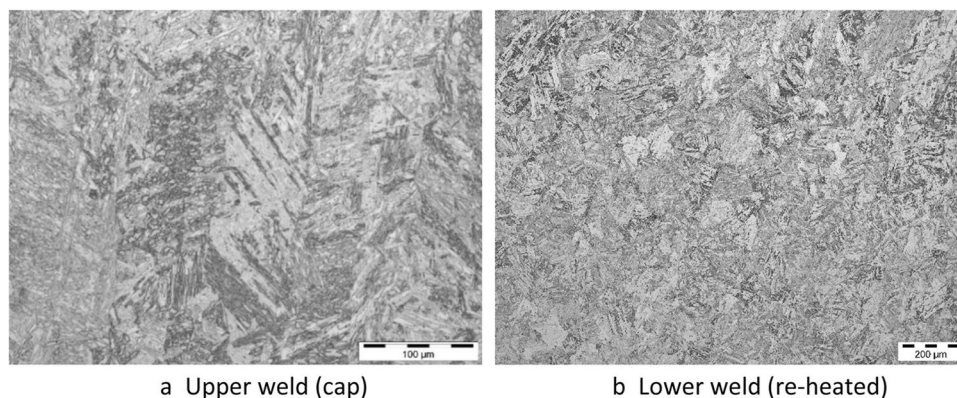
Figure 5 shows BSE micrographs after different PWHT holding times, in which the bright precipitates, Laves phase, within the upper and lower weld regions are clearly visible. The size and distribution of the Laves phase present in the weld metals changes significantly with increased heat treatment duration.

After 8 h, small Laves phase precipitates are present, mainly on grain and sub-grain boundaries.

After 16 h, Laves phase precipitates are more apparent. They appear larger than those after 8 h at 735 °C. The increased time at temperature has caused more Laves phase to precipitate as demonstrated by an apparent increase in their size.

After 36 h, fewer Laves phase precipitates are present; however, the ones that are present appear to be significantly larger after 16 h at 735 °C. This observation of coarsening is consistent with previous data from P92 which showed that maximum Laves particle size was obtained between 10 and 20 h of thermal exposure at 600 and 650 °C, respectively [23]. The precipitates are also more clustered in certain areas and around certain boundaries whereas after 16 h of heat treatment, the precipitates are more evenly distributed by comparison. This means

Fig. 3 Microstructure of the weld in as-welded condition



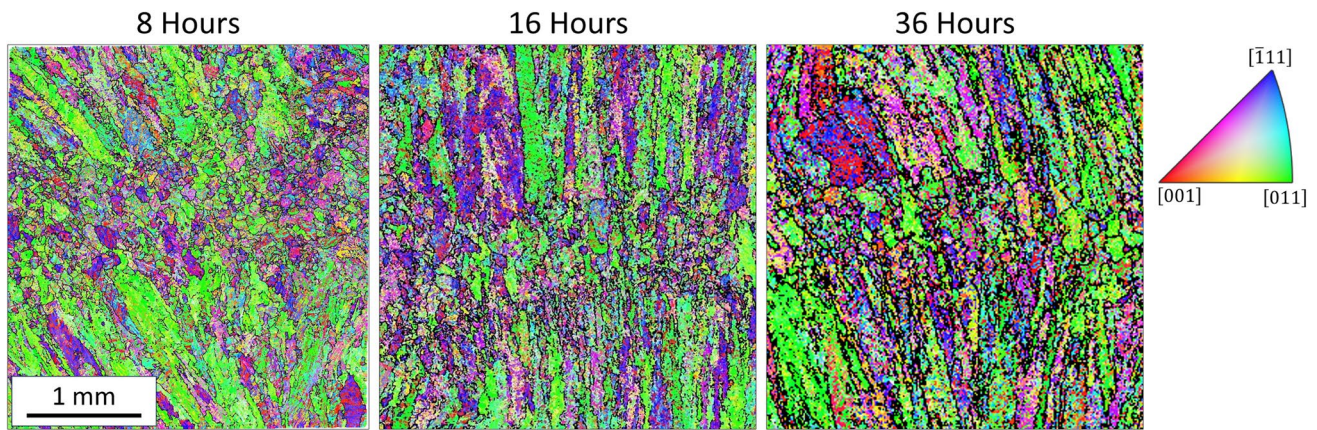


Fig. 4 EBSD Maps of the microstructure of the weld after PWHT 735 °C×8, 16 and 36 h

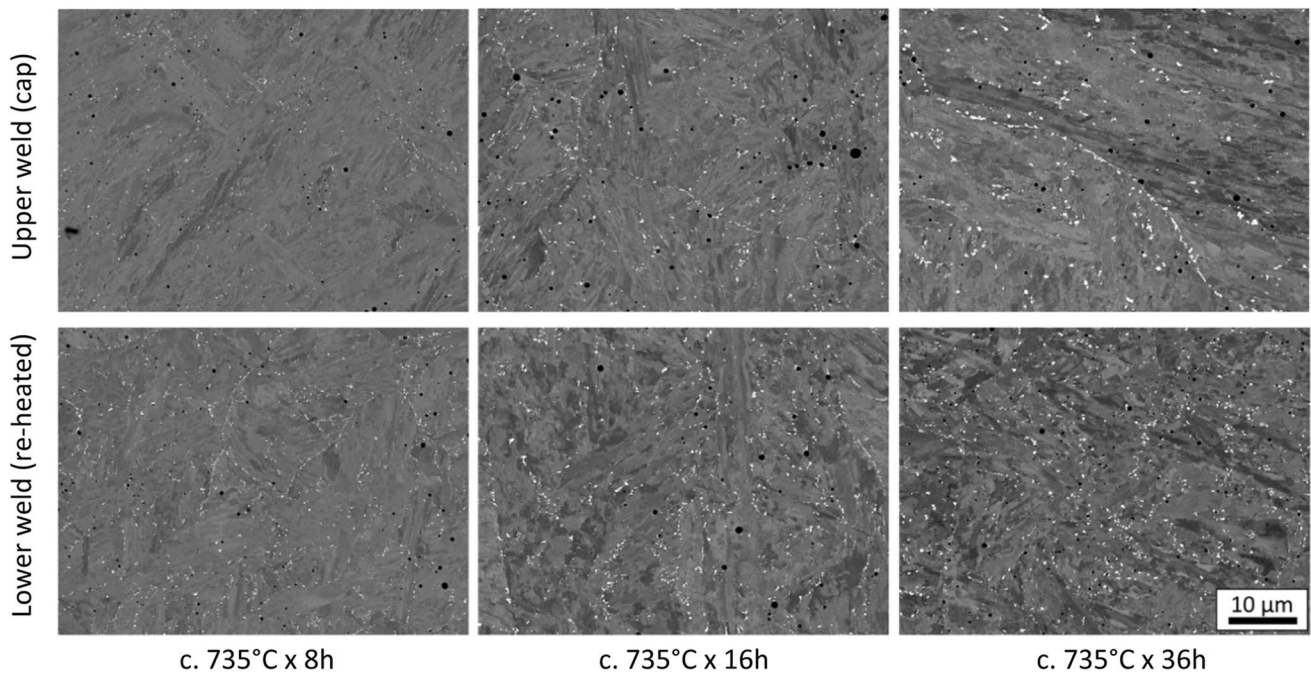


Fig. 5 BSE images of upper (cap) and lower (re-heated) weld regions after PWHT 735 °C×8, 16 and 36 h

that at a certain point of heat treatment, the Laves phase present has reached a relatively stable volume fraction, so instead of precipitation of new precipitates, the dominant mode has changed to coarsening of the precipitates present, where larger precipitates increase in size and consume smaller precipitates, leaving fewer larger precipitates as a result with a similar volume fraction.

In order to balance the beneficial effects of PWHT on the ambient properties against long-term creep-performance, it is recommended that any PWHT be limited to minimize coarsening of precipitates. This ensures that the Laves phase particles remain as small as possible whilst also realizing

the beneficial effects of the improved mechanical properties after PWHT.

There is also a difference in the precipitation between weld regions. There are differences in precipitate size and distributions between the weld cap region and central region (upper and lower regions, respectively). Figure 6 shows that the lower weld central regions have a greater density of Laves precipitates compared to the cap regions, an observation which is confirmed by the following quantitative analysis.

Figure 7 shows the full particle size data plotted as both number-weighted and area-weighted particle size

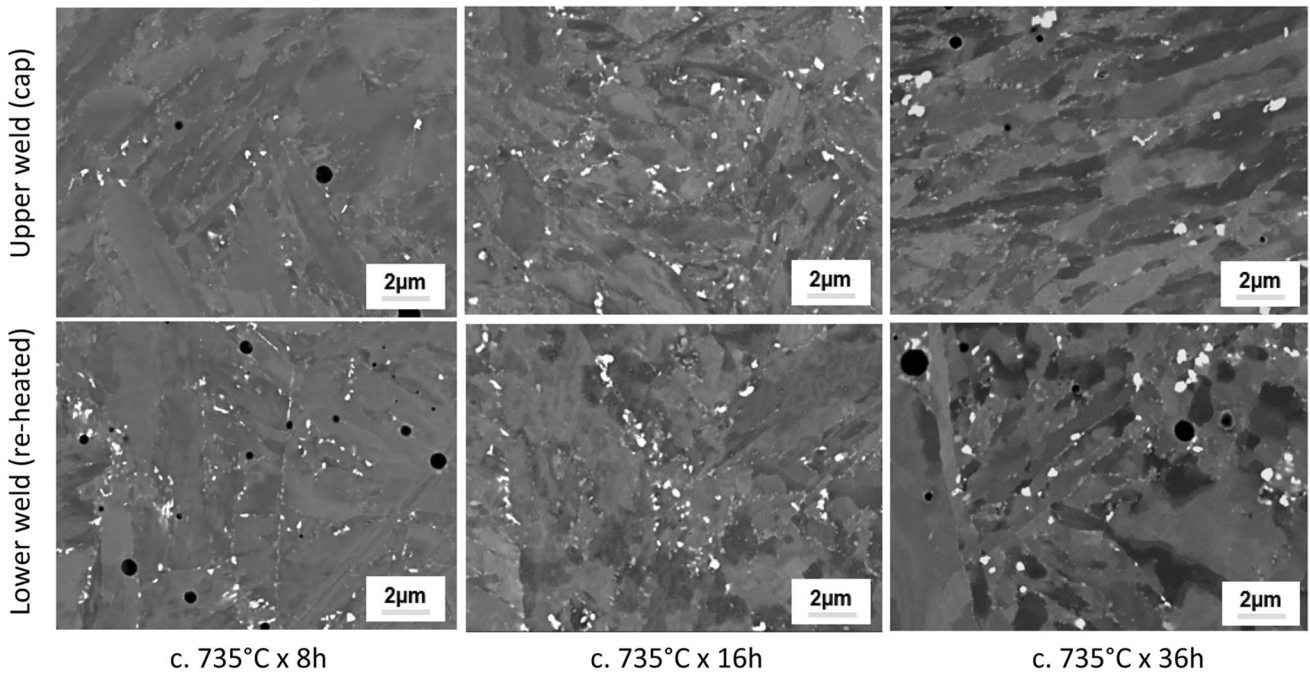


Fig.6 PWHT 735 °C: Laves precipitation vs duration—difference in weld regions

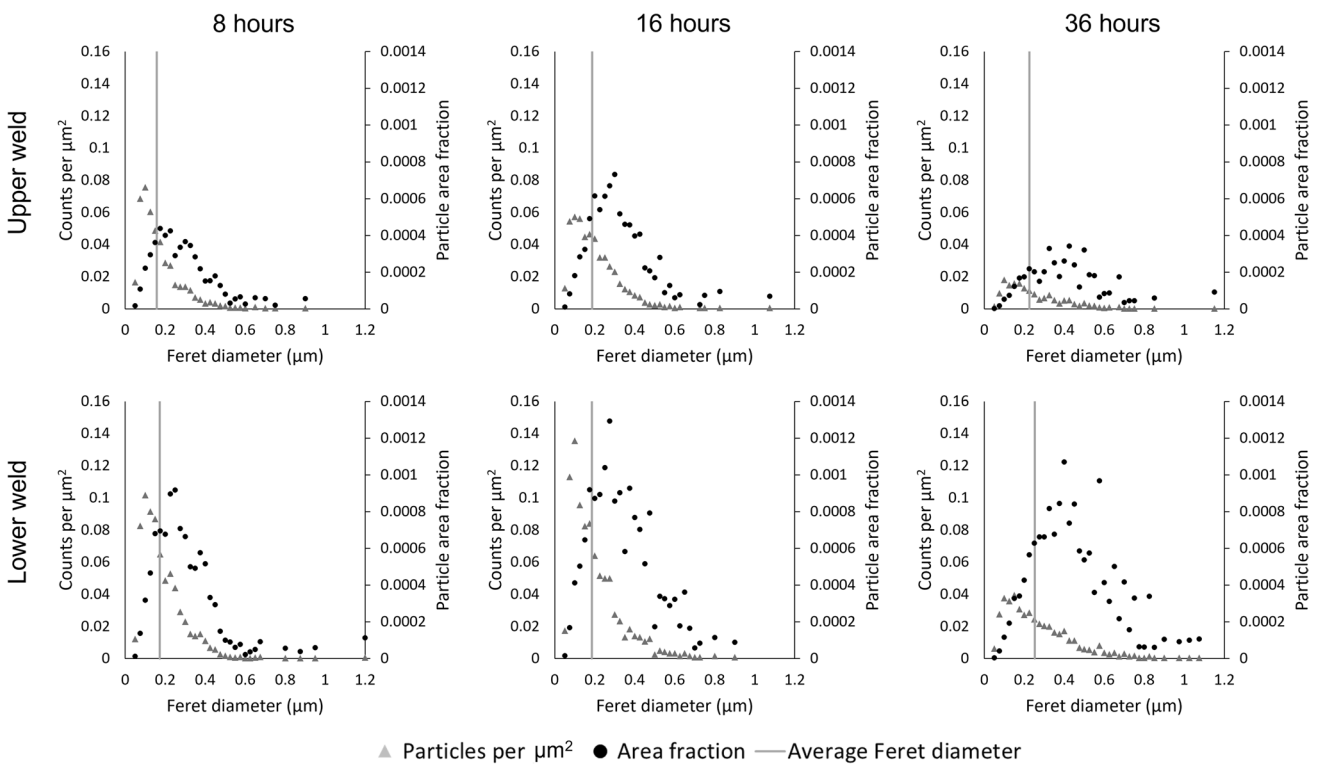


Fig. 7 Particle size distributions for the all-weld metal samples with different PWHTs from the upper and lower weld metal regions

distributions. These plots show the evolving laves particle sizes as a function of PWHT time. In the upper section of the weld, the area fraction of laves increases from 8 to 16 h

PWHT time, with an associated decrease in the number of particles per μm². After 36 h, both the count and area fraction appear to fall, but the Feret diameter has increased

Table 4 Quantification analysis of the Laves phase precipitations: weld locations and holding time

Duration/location	Average area (μm^2)	Average Feret diameter (μm)	Area percentage (%)	Counts per area (μm^{-2})
8 h upper (cap)	0.0097	0.137	0.41	0.485
8 h lower (re-heated)	0.0129	0.160	1.10	0.878
16 h upper (cap)	0.0139	0.162	0.81	0.583
16 h lower (cap)	0.0150	0.158	1.55	1.166
36 h upper (cap)	0.0330	0.214	1.03	0.313
36 h lower (re-heated)	0.0259	0.191	1.50	0.605

which leads to a similar area fraction of Laves between 16 and 36 h hold (Table 4). The average particle Feret diameter increases with hold-time. For the lower part of the weld, the area fraction is consistently higher than the upper section. However, the number of particles decreases after 36 h PWHT time. Again, the average Feret diameter also increases with hold-time.

Table 4 gives an assessment of the average data from the quantitative assessment of the Laves phase precipitates within the structure. The results are plotted in Figs. 8, 9 and 10. The analysis indicates that the bright particles have begun to coarsen with the holding time of 36 h at 735 °C, as indicated by a reduction in the counts per unit area, increase in average precipitate size and stabilisation of total area percentage.

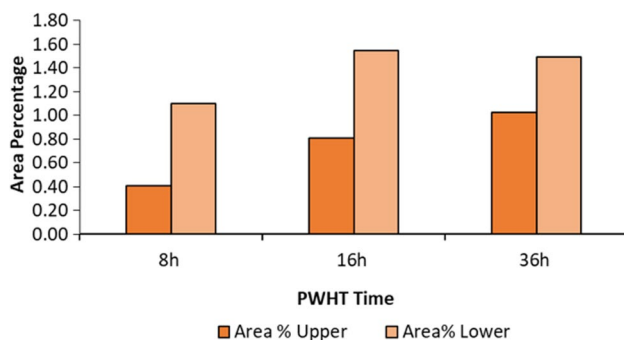
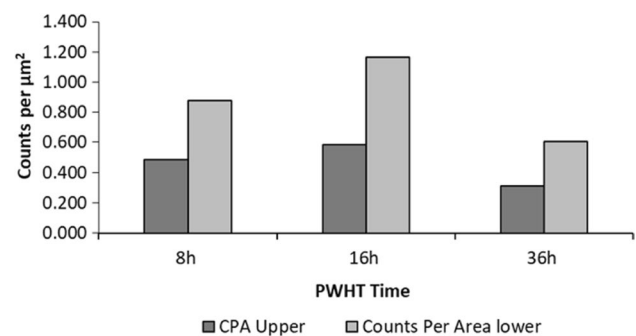
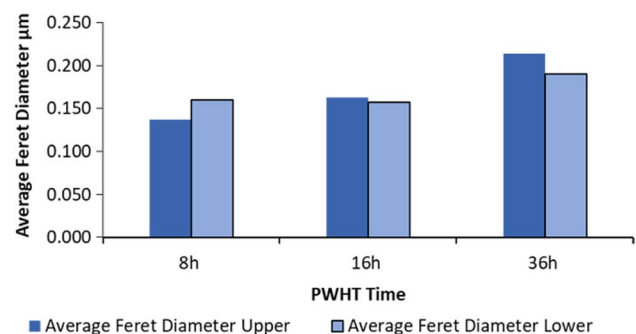
Figure 11 compares the presence of M_{23}C_6 carbides precipitates (the grey particles visible as indicated by the arrows) after different PWHT holding times. From the images, the M_{23}C_6 carbides appear to follow a similar trend to the Laves phase through the different durations of PWHT, although this has not been quantified in this study.

After 8 h, there are a small number of medium sized carbides and slightly more smaller carbides present on some sub-grain boundaries in the material. After 16 h of heat treatment the carbides appear more abundant in general although similar in size to those present after 8 h. After 36 h, there are a number of significantly larger carbides present along

with a number of smaller carbides, but potentially less in total than after 16 h.

Therefore, it seems that between 8 and 16 h, many more carbides have precipitated and reached a particular size, but not many have grown significantly more than that. Whereas between 16 and 26 h, it appears that coarsening may be occurring, with a number of carbides growing larger and the smaller carbides potentially being consumed by the larger carbides.

Coarsening of the carbides will potentially reduce their strengthening effect on the material, and therefore, it appears that heat treating the material for more than 16 h at 735 °C does not impart any extra benefit and may in fact negatively affect the mechanical properties if the coarsening of the carbides is significant. This observation appears to be in

**Fig. 8** Quantification analysis of Laves phase. Area percentage**Fig. 9** Quantification analysis of Laves phase. Count per μm^2 **Fig. 10** Quantification analysis of Laves phase: average Feret diameter

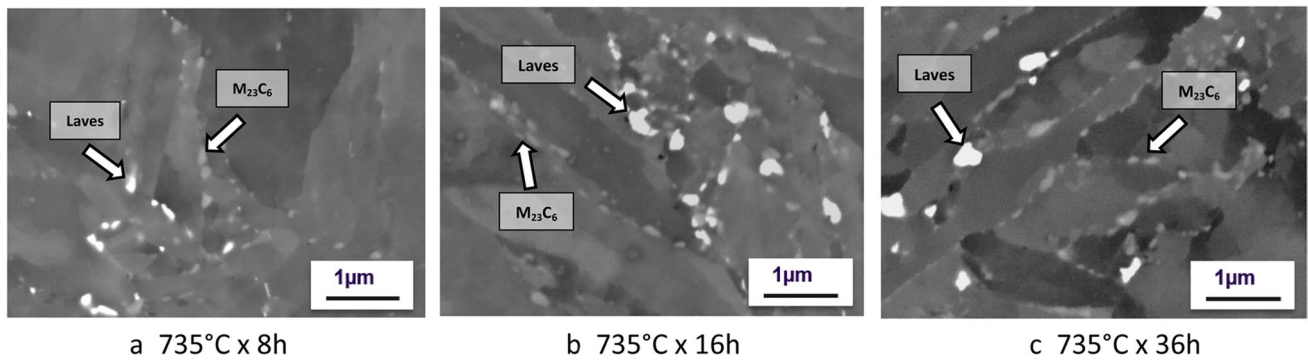
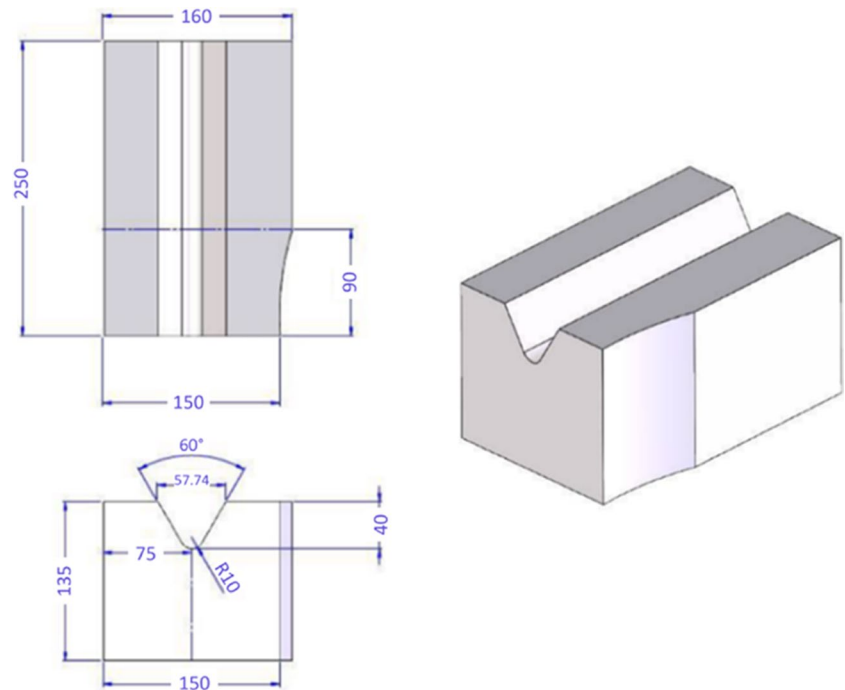


Fig. 11 PWHT 735 °C: effect of duration on precipitations– $M_{23}C_6$ carbides

Fig. 12 The geometry and dimensions of the U-groove weld block in IBN-1 casting



agreement with the slightly lowered weld tensile strength as the PWHT time extended over 16 h.

3.2 IBN-1 casting weld joint test and results

3.2.1 Welding of cast joint and PWHT

Weld joints in cast IBN-1 were prepared to evaluate the cross-weld properties and the effect of PWHT and welding procedure. A U-groove weld joint machined from a 135 mm × 150 mm × 250 mm IBN-1 cast block was used

for the casting joint test. The dimensions of the joint are illustrated in Fig. 12.

Electrodes of diameters 3.2 mm and 4.0 mm were used. The welding parameters used were voltage 24 V and current 110 A with a heat input of ~ 1.1 kJ/mm for dia 3.2 mm electrode and 25 V 140 A with a heat input of ~ 1.3 kJ/mm for diameter 4.0 mm electrode. The weld was filled with the 3.2 mm electrode for the first 20% of the joint groove height (approximately 8–10 mm) and the remaining 80% height (approximately 35–37 mm) was filled with the 4.0 mm electrode.

Table 5 Transverse tensile test and side bend test of weld joint after different PWHT

Material	Interpass temperature	PWHT	Rm (MPa)	Z (%)	Fracture location	Fracture type	Side bend test
IBN-1 [8]	NA	Annealed + tempered	767	60	NA ^a	NA ^a	NA ^a
IBN-1 casting weld joint	350 °C	735 °C × 8 h + FC	786	49	Base metal	Ductile	Acceptable
			771	46	Base metal	Ductile	Acceptable
			782	46	Base metal	Ductile	Acceptable
			798	55	Base metal	Ductile	Acceptable
		735 °C × 16 h + FC	805	48	Base metal	Ductile	Acceptable
			773	54	Base metal	Ductile	Acceptable
			805	52	Base metal	Ductile	Acceptable
			777	51	Base metal	Ductile	Acceptable

NA not applicable

The pre-heat temperature was 150 °C. Two different interpass temperatures, 350 °C and 250 °C, were used to explore the effect. The weld joints were cooled down to <80 °C, then post-weld hydrogen baking was carried out at 320 °C for 6 h, followed by the different PWHTs.

Considering that, in the all-weld metal tests, PWHT at 735 °C with holding durations of 8 h and 16 h achieved optimum impact toughness, the PWHT for the casting joint tests started with these parameters.

3.2.2 Mechanical properties of the casting joint and effect of inter pass temperature and PWHT

Table 5 lists the results of cross-weld transverse tensile tests and side bend tests of the weld joint with an interpass temperature of 350 °C. Four specimens for each PWHT were tested. The tensile specimens were all ruptured in the weld heat affected zone (HAZ). All samples showed ductile fracture. The strength values were slightly higher than the typical IBN-1 base metal level, and the reduction of area data were slightly lower than the base metal, similar to those

obtained from the weld metal deposit test. Side bend tests were all passed without indication of defects.

Charpy impact tests were carried out at 20 °C with notch locations at the weld centreline, HAZ regions 3 mm and 5 mm away from the fusion line. The results are listed in Table 6. The values of absorbed impact energy from the samples after 735 °C × 16 h were in line with those achieved by the all-weld metal tests after PWHT at 735 °C × 8, 16 and 32 h. However, the toughness after PWHT at 735 °C × 8 h was substantially lower. Two factors are considered as the reasons for this, and the effect could be the combination of both. The first effect is that the considerably large volume of the IBN-1 cast block used for the groove joint may mean that an 8 h hold is insufficient to achieve an adequate tempering effect. The second possibility could be that 8 h heat treatment did not reach the robustly stable tempering effect, hence inconsistencies between the different tests. Holding for 16 h on the other hand has reached a stable and thorough tempering effect; hence, it produced consistent properties (Table 6).

Table 6 Charpy impact test of weld joint with different interpass temperatures and PWHTs

Material	Interpass temperature	PWHT	Location	CVN at +20 °C J, avg./ind
IBN-1 cast weld joint	350 °C	735 °C × 8 h + FC	Weld metal	8/6, 8, 10
			Fusion line + 3 mm	15/20, 10, 14
			Fusion line + 5 mm	14/21, 16, 6
		735 °C × 16 h + FC	Weld metal	27/34, 24, 22
			Fusion line + 3 mm	32/24, 33, 37
			Fusion line + 5 mm	32/29, 29, 38
	250 °C	735 °C × 16 h + FC	Weld metal	39/54, 34, 28
			Fusion line + 3 mm	32/31, 24, 42
			735 °C × 36 h + FC	Weld metal
Fusion line + 3 mm	28/32, 27, 26			

Welding with an interpass temperature of 250 °C demonstrated considerably better toughness than welding with a 350 °C interpass temperature, while the toughness of the HAZ region was identical. Again, a further increase in holding time from 16 to 36 h did not show further addition of toughness.

Cross-weld transverse hardness surveys were conducted of the weld joints covering the regions of base metal–HAZ–weld–HAZ–base metal. The results are plotted in Figs. 13 and 14. From Fig. 13, it can be seen, that after 8 h holding at 735 °C, the weld still had a hardness above 300 HV. After 16 h holding, a substantial tempering effect was achieved, and the weld hardness lowered to a similar level to those of the base metal regions. This agrees with the speculation of less adequate tempering effect of 8 h, hence lower impact toughness. Figure 13 compares the hardness distributions of the weld joints from interpass temperatures of 250 and 350 °C after PWHT at 735 °C × 16 h. It shows that in the regions of weld and HAZ, the hardness of the joint welded with interpass temperature 250 °C is slightly lower than that the one using 350 °C.

3.2.3 Microstructure examination of the weld joint and effect of interpass temperature and PWHT

Figure 15 shows the EBSD maps of the weld joint microstructure from a high (350 °C) and a low (250 °C) interpass temperature after PWHT at 735 °C for 16 h, which show no obvious differences in the grain structure of the weld or HAZ regions between the two interpass temperatures. From these maps, the HAZ can be seen to have a structure as previously observed [9] where fine grains are present around the edge of the larger prior austenite grains in this region.

Figure 16 shows the BSE images of the microstructure of the two weld metals focusing on the presence of high contrast particles within the structure which are again considered to be Laves phase particles. It can be seen that these particles are present in all areas of the weld joint, i.e. weld metal, fusion line and HAZ, along lath and prior austenite grain (PAG) boundaries. Within the weld metal at both interpass temperatures, dark circular features were observed which are inclusions formed from the welding process.

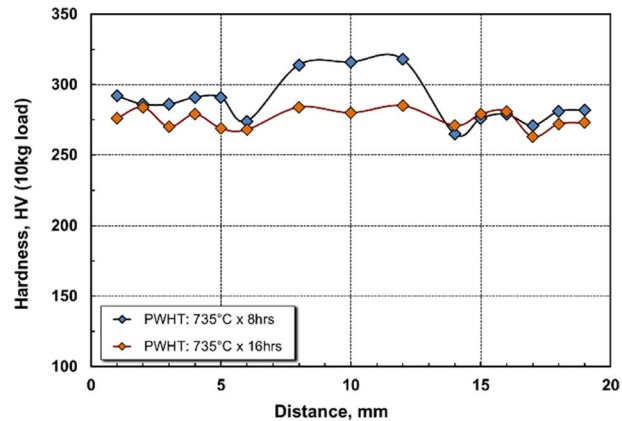
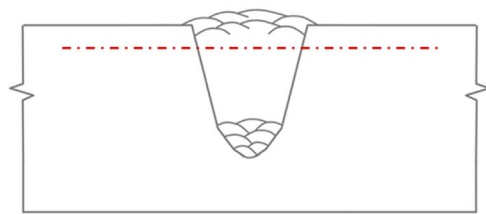


Fig. 13 Cross-weld HV survey (interpass temperature = 350 °C) (PWHT: 735 °C × 8 h vs 735 °C × 16 h)

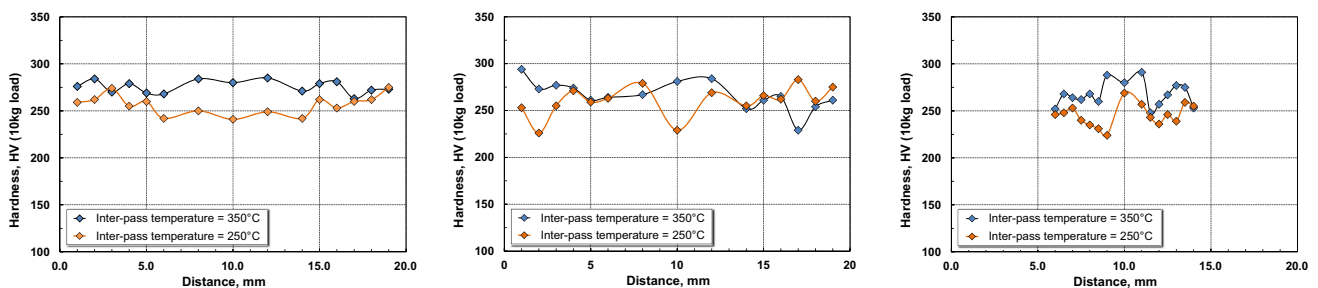


Fig. 14 Cross-weld HV survey (interpass temperature: 250 °C vs 350 °C) (PWHT: 735 °C × 16 h)

Fig. 15 EBSD maps of the microstructure of the weld joint area (PWHT: 735 °C × 16 h)

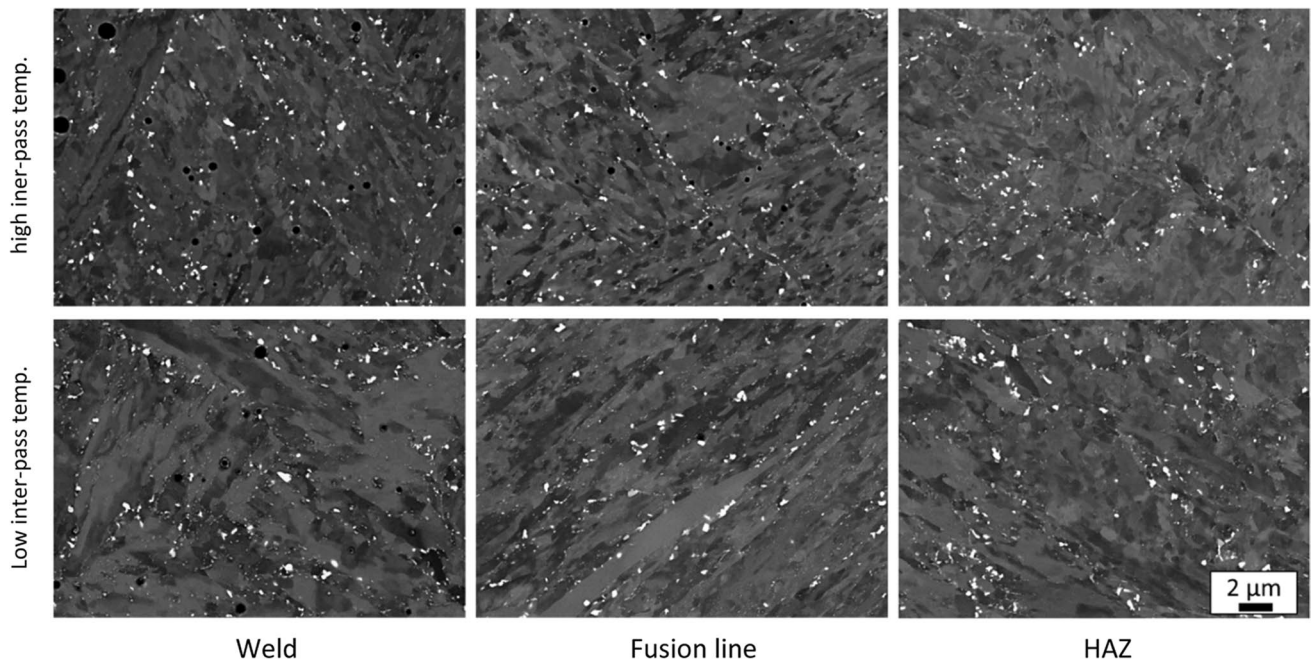
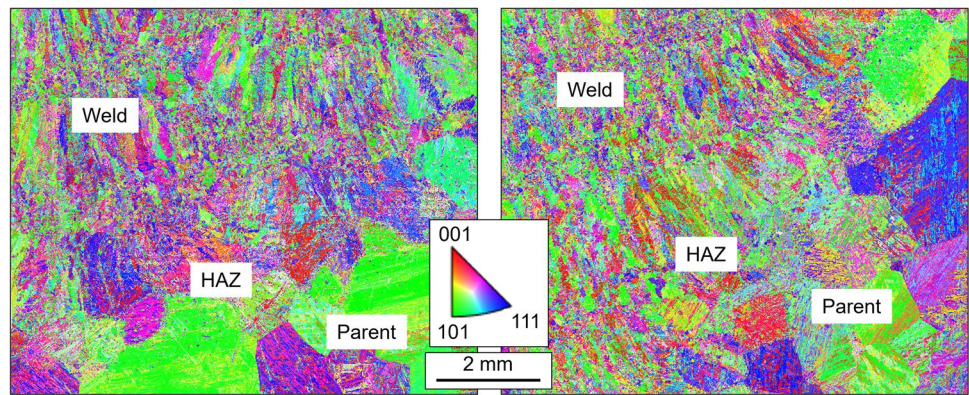


Fig. 16 BSE images showing Laves precipitation within different regions of the joint (PWHT 735 °C × 16 h)

On quantification of the bright particles within the weld metal, the data shown in Fig. 17 can be extracted. It is apparent that there are a greater number of particles per μm^2 in the higher interpass temperature condition compared to the lower interpass temperature (1.12 vs 0.69 particle per μm^2 respectively) and that there are also a greater population of particles with a smaller area within the higher interpass temperature weld metal. It is likely that this difference in Laves phase precipitation relates to the weld impact toughness variation between high and low interpass temperatures. However, the effect of the presence of these different size populations of laves phase is unclear. Further analysis is required to establish whether there are any differences in other microstructural features such as carbide populations in the different weld areas.

4 Summary

The matching welding consumable for IBN-1 MarBN steel was evaluated in order to develop an appropriate welding procedure to join cast components which require a lower PWHT temperature. Using all-weld metal coupons and IBN-1 casting welded joints, the influences of PWHT and welding interpass temperature were investigated. Mechanical tests and microstructure analysis were conducted. The results obtained at this stage can be summarised as below:-

- With a 30 mm thick all-weld metal coupon, reasonable impact toughness was achieved after PWHT

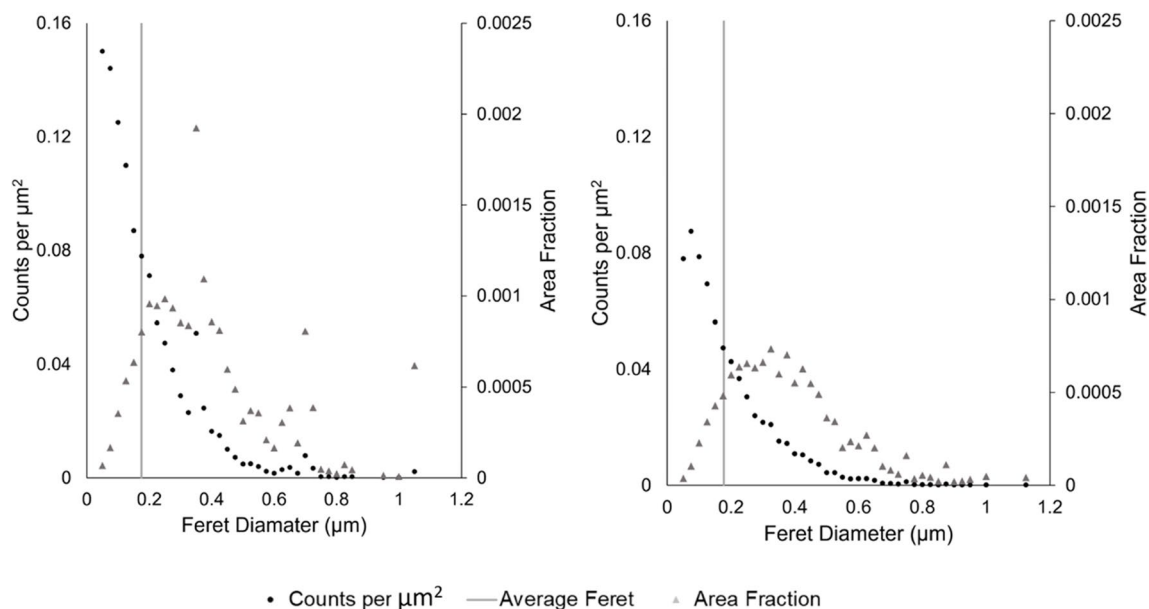


Fig. 17 Counts of precipitation particles in weld metals from high and low interpass temperatures

735 °C × 8 h; longer heat treatment durations (16 h and 36 h) did not further increase the toughness.

- For thicker cast blocks, a PWHT of 735 °C × 16 h was needed to produce a weld toughness comparable to the base metal. The hardness survey indicated the weld was not adequately tempered after 8 h, indicating that for an actual engineering application, PWHT at 735 °C with a 16 h hold is appropriate for large cast components.
- Test data showed that a lower interpass temperature of 250 °C produced better and more consistent toughness than higher interpass temperature of 350 °C; longer PWHT durations (36 h) did not further increase the toughness.
- Evenly distributed Laves phase precipitation was observed after 735 °C × 8 h in the all-weld coupon; the precipitation gradually increased in size and area fraction as the duration increased (16 h and 36 h); and appeared to be stable when approaching 36 h.
- A difference in the precipitation was observed between different weld regions. The weld cap region which experiences lower or no reheating, had a lower density of Laves precipitates compared to lower weld area where reheating was applied to the microstructure by the subsequent welding passes.

authors acknowledge use of the facilities and the assistance of Sam Davis and Dr Stuart Robertson in the Loughborough Materials Characterisation Centre (LMCC) and for access to the Helios PFIB, funded by the EPSRC grant EP/P030599/1.

Funding This study is funded by Innovate UK, under Project IMPLANT: “Advanced Materials and Manufacturing for Improved Power and Process Plant Performance”, Innovate UK File Ref. 105769, Jan 2020–April 2022, and their other project partners: Uniper Technologies Limited, University of Birmingham, ETD Consulting UK.

Data availability The data used to create the particle size data in this paper are available from the Loughborough University repository and can be found at the following <https://doi.org/10.17028/rd.lboro.24614109>.

Declarations

Competing interests The authors declare no competing interests.

Open Access This article is licensed under a Creative Commons Attribution 4.0 International License, which permits use, sharing, adaptation, distribution and reproduction in any medium or format, as long as you give appropriate credit to the original author(s) and the source, provide a link to the Creative Commons licence, and indicate if changes were made. The images or other third party material in this article are included in the article’s Creative Commons licence, unless indicated otherwise in a credit line to the material. If material is not included in the article’s Creative Commons licence and your intended use is not permitted by statutory regulation or exceeds the permitted use, you will need to obtain permission directly from the copyright holder. To view a copy of this licence, visit <http://creativecommons.org/licenses/by/4.0/>.

Acknowledgements The authors gratefully acknowledge Dr David Allen for his contribution in relation to welding parameters. The

References

- Abe F, Horiuchi B, Teneike M, Okada K (2004) Stabilization of martensitic microstructure in advanced 9Cr steel during creep at high temperature. *Mater Sci Eng, A* 378:299–303
- Albert SK, Kondo M, Tabuchi M, Yin F, Sawada K, Abe F (2005) Improving the creep properties of 9Cr-3W-3Co-NbV steels and their weld joints by the addition of boron. *Metall Mater Trans A* 36(2):333–343
- Abe F (2006) Metallurgy for long-term stabilization of ferritic steels for thick section boiler components in USC power plant at 650°C. In: Lecomte-Beckers J, Carton M, Schubert F, Ennis PJ (eds) Conference proceedings: materials for advanced power engineering. Julich, Belgium, pp 965–980
- IMPACT Project. Innovative materials, design and monitoring of power plant to accommodate carbon capture. A UK Technology Strategy Board (TSB) funded collaborative R&D project, Dec 2009 – Dec 2013
- Hamaguchi T, Okada H, Kurihara S, Hirata H, Yoshizawa M, Iseda A (2017) Microstructural evaluation of 9Cr-3W-3Co-Nd-B heat-resistant steel (SAVE12AD) after long-term creep deformation. Proceedings of the ASME 2017 Pressure Vessels and Piping Conference PVP2017, PVP2017-65241, Waikoloa, Hawaii, USA, 16–20 July 2017
- IMPEL Project. A UK collaborative project for feasibility studies of MarBN base alloy and filler metal, 2014 – 2019
- IMPULSE Project. Advanced industrial manufacture of next-generation marbn steel for cleaner fossil plant. Innovate UK File Ref. 102468, May 2016 – April 2019
- Roberts S, Leese R, Birks S (2019) The status of continued development of heavy section casting in 9%Cr steels and nickel alloys for high temperature applications. Joint EPRI-123HIMAT Int. Conference on Advances in High Temperature Materials, Nagasaki, Japan, 21–25 October 2019
- Guo J, Xu X, Jepson MAE, Thomson RC (2019) Influence of weld thermal cycle and post weld heat treatment on the microstructure of MarBN steel. *Int J Press Vessels Pip* 174:13–24
- Lockyer SA, Jepson MAE, Xu X, Philpott W (2019) Microstructure analysis of service exposed IBN1 MarBN steel boiler tubing. Joint EPRI-123HIMAT International Conference on Advances in High Temperature materials, Nagasaki, Japan, 21–25 October 2019
- Zhang Z, Mee VvD (2021) Development of the matching filler metal for MarBN – new advanced creep resisting alloys for thermal power plant. *Weld World* 65(4):1599–1608
- Zhang Z, Mee VvD, Allen D (2021) Assessment of deposit microstructure and all-weld and joint creep performance of the matching filler metal for the MarBN alloys. *Mater High Temp*
- IMPLANT Project. Advanced materials and manufacturing for improved power and process plant performance. Innovate UK File Ref. 105769, Jan 2020 – Dec 2022
- Abe F (2005) Effect of fine precipitation and subsequent coarsening of Fe₂W laves phase on the creep formation behavior of tempered martensitic 9Cr-W steels. *Metall Mater Trans A* 36A:321–332
- AWS Specification A5.5/A5.5M:2014 (An American National Standard) (2014) Specification for lowalloy steel electrodes for shielded metal arc welding. American Welding Society
- EN ISO 3580:2017 (2017) Welding consumables - Covered electrodes for manual metal arc welding of creep-resisting steels – Classification. Technical Committee ISO/TC44
- Swindeman RW, Santella ML, Maziasz PJ, Roberts BW, Coleman K (2004) Issues in replacing Cr-Mo steels and stainless steels with 9Cr-1Mo-V steel. *Int J Press Vessel Pip* 8(6):507–512
- Spigarelli S, Evangelista E, Mehtedi ME, Balloni L, Poli A (2005) Analysis of effect of chemical composition on hot forming operations of P91 steel. 1st International Conference Super-high Strength Steels, Rome, Italy, 2–4 November 2005
- ASTM E8/E8M-16a (2016) Standard test methods for tension testing of metallic materials. ASTM Int
- ASTM E10-18 (2018) Standard test method for brinell hardness of metallic materials. ASTM Int
- ASTM A370-19 (2019) Standard test methods and definitions for mechanical testing of steel products. ASTM Int
- ASTM E190-14 (2014) Standard test method for guided bend test for ductility of welds. ASTM Int
- Hald J (2008) Microstructure and long-term creep properties of 9–12% Cr steels. *Int J Press Vessels Pip* 85:30–37

Publisher's Note Springer Nature remains neutral with regard to jurisdictional claims in published maps and institutional affiliations.